Available online at www.sciencedirect.com
ScienceDirect
Ceramics International 37 (2011) 1191–1201
CERAMICS INTERNATIONAL
www.elsevier.com/locate/ceramint

Thermodynamic evaluation of spinel containing refractory castables corrosion by secondary metallurgy slag

A.P. Luz [a,*], A.G. Tomba Martinez [b], M.A.L. Braulio [a], V.C. Pandolfelli [a]

[a] Federal University of São Carlos – Materials Engineering Department, Rod. Washington Luiz, km 235, São Carlos – SP, C.P. 676, CEP 13565-905, Brazil
[b] Materials Science and Technology Research Institute (INTEMA), Ceramics Division, Av. Juan B. Justo 4302, (7600) Mar del Plata, Argentina

Received 24 July 2010; received in revised form 23 October 2010; accepted 28 November 2010
Available online 21 January 2011

Abstract

This work addresses the thermodynamic evaluation of different spinel-containing refractory castable compositions in contact with a basic steel ladle slag ($CaO/SiO_2 \sim 9$). The main differences among the castable compositions were the amount of silica fume (0 or 1 wt%), the binder source (calcium aluminate cement or hydratable alumina) and the spinel incorporation route (*in situ* or pre-formed). The interaction of the liquid slag with the refractory was carried out with the help of thermodynamic software (FactSage) and the applied methodology considered the changes in the slag composition due to the interaction with the castable. The theoretical results were compared with the experimental data attained by corrosion cup-tests, pointing out that the thermodynamic calculations were suitable for predicting various aspects observed in the corroded samples by SEM. Therefore, the equilibrium simulations led to parameters that indicated the corrosion resistance trends, complementing the experimental evaluation and reducing further experimental testing.

Keywords: C. Corrosion; Spinel containing castables; Thermodynamic simulation; Spinel

1. Introduction

Corrosion of spinel containing castables has been extensively studied [1–6]. Nevertheless, although work has been reported on the dissolution of Al_2O_3 into lime–alumina–silica slags [7–9], information regarding the reaction mechanisms and the characterization of the formed phases in the refractories microstructure at high temperatures is rather limited.

Al_2O_3–$MgAl_2O_4$ refractory castables present higher resistance to structural spalling than high alumina or basic castables due to their lower slag penetration. Refractory compositions in this system can be designed based on adding [9,10]: (a) coarse pre-formed spinel grains as aggregates, (b) fine pre-formed spinel as one of the constituents of the castable matrix, and (c) MgO and Al_2O_3 fines in order to generate the *in situ* spinel phase. Some authors [1,5] stated that fine spinel, formed *in situ* by the reaction of MgO and Al_2O_3 in the castable matrix, increases the slag penetration resistance when compared to pre-formed spinel containing ones. The positive effect of the *in situ* spinel formation on the refractory corrosion performance is still under discussion in the scientific literature. Sarpoolaky et al. [9] consider that the corrosion resistance of the spinel containing castables is mainly associated with the extensive interlocking between calcium hexaluminate ($CaO{\cdot}6Al_2O_3$ – formed due to the transformations and reactions of the calcium aluminate cement used as the bonding additive) and corundum or spinel grains in the matrix of the castables.

On the other hand, because the slag is the most reactive component in the melt, its composition has a critical effect on the corrosion mechanism of the Al_2O_3–$MgAl_2O_4$ refractories [1,10]. The current knowledge and understanding of the reaction sequences involved in the dissolution of alumina and spinel in the molten slags, particularly the nature of the various formed phases at the slag/castable interface and their stability regarding the slag composition and heat treatment temperature, are far from being complete [7,11].

Due to these aspects, an alternative to understand the reaction and corrosion mechanisms of the spinel containing castables and to predict their phase evolution at a high temperature is the thermodynamic calculations. The FactSage

* Corresponding author. Tel.: +55 16 33518253; fax: +55 16 33615404.
E-mail address: anapaula.light@gmail.com (A.P. Luz).

0272-8842/$36.00
doi:10.1016/j.ceramint.2010.11.043

software is an important tool to perform a wide range of thermochemical calculations. It provides information on the formed phases, their proportions and compositions, the chemical activities of individual components and the thermodynamic properties for the compositions at different partial pressures and temperatures [12].

Recently, some studies on the prediction of castable corrosion behavior were undertaken, considering the FactSage thermodynamic modeling [13,14]. Although very important insights could be attained in these works, some important factors, such as the saturation of the slag by the castable components and its chemical composition change after the reaction with the refractory, were not considered in these calculations [14]. Thus, some improvements in the thermodynamic modeling are still required to better fit the severe conditions that these refractories are exposed to during experimental tests and practical use.

This work addresses the evaluation of the corrosion mechanisms and phase formation of four spinel containing refractory castables when in contact with a selected industrial secondary metallurgy slag composition. Additionally, the effect of silica fume, the binder source (in alumina–magnesia refractory castables) and also the spinel incorporation method (*in situ* versus pre-formed for CAC and silica fume-containing compositions) were analysed. A novel thermodynamic modeling was proposed and successive calculations were applied, considering the liquid composition changes during the interaction with solid phases at 1550 °C. Moreover, in order to point out the advantages and odds of the thermodynamic analyses, experimental corrosion cup tests were also carried out and these results were further compared with the calculated ones.

2. Experimental

2.1. Refractory castable compositions

Four vibratable castables were designed using the Alfred particle packing model ($q = 0.26$). Coarse tabular alumina was used as aggregate ($d \leq 6$ mm, Almatis, USA) and the castable matrix was comprised by dead-burnt magnesia ($d < 45$ μm, 95 wt% of MgO, $CaO/SiO_2 = 0.37$, Magnesita Refratários S.A., Brazil), silica fume (971U, Elkem, Norway), reactive alumina (CL370, Almatis, USA) and fine tabular alumina ($d < 200$ μm, Almatis, USA). General information regarding the compositions is presented in Table 1.

Two binders were selected and a total of 6 wt% of them was added to the castables: calcium aluminate cement CAC (Secar 71, Kerneos, France) or hydratable alumina HA (AlphaBond 300, Almatis, USA). An additional composition, PF-6C1S (Table 1), containing aggregates and fine particles of pre-formed $MgAl_2O_4$ spinel (78 wt% of Al_2O_3, $d < 1$ mm, Almatis, USA), was also evaluated. The addition of pre-formed spinel in this castable aimed to analyse the role and the resulting differences between this sort of spinel addition and the *in situ* spinel formation in the castable corrosion behavior.

2.2. Thermodynamic simulations

The calculations performed in this work were based on the minimization of the free energy of the system in order to find out the nature of the solid, liquid and gaseous phases, as well as their chemical composition and reaction rate at the thermodynamic equilibrium [12]. Simulations have been carried out using FactSage (version 6.1), a fully integrated database and software jointly developed between Thermfact/CRCT (Montreal) and GTT-Technologies (Aachen). It consists of a series of modules that access and cross link thermodynamic databases and allow various calculations.

The databases used in this study were: Fact53 and SGTE (gaseous species, solid and liquid compound thermodynamic database) and FToxid (compounds and solutions for oxide databases). The equilibrium phases were predicted using the Equilib module, considering the following as possible phases: gas, slag or liquid and various solid-solutions (including spinel, mullite, etc.).

There are several procedures in the thermodynamic calculations that can be applied for evaluating the corrosion behavior of the refractory materials. A corrosion modeling proposed by Berjonneau et al. [14] includes the analysis of the refractory (R) and the slag (S) contact at a constant temperature and pressure, where all possible proportions (in mass) between these two materials are studied as a function of the reaction rate <A>, which is defined by the ratio: $(R)/[(S) + (R)]$ with

Table 1
General information of the castables compositions.

Designed compositions		IS-6C1S	IS-6C0S	IS-6H1S	PF-6C1S
Raw Materials	Tabular ($d < 3$ mm) and reactive alumina ($d_{50} = 4$ μm)	87	88	93	72
	Dead-burnt magnesia ($d < 45$ μm)	6	6	6	–
	Calcium aluminate cement	6	6	–	6
	Hydratable alumina	–	–	6	–
	Silica fume	1	–	1	1
	Pre-formed spinel ($d < 1$ mm)	–	–	–	21
Chemical composition	Al_2O_3	91.2	92.2	93.0	91.2
	MgO	6.0	6.0	6.0	6.0
	CaO	1.8	1.8	–	1.8
	SiO_2	1.0	–	1.0	1.0

IS: *in situ* spinel formation. 6C or 6H: 6 wt% calcium aluminate cement or hydratable alumina, respectively. 1S or 0S: 1 wt% or 0 wt% of silica fume, respectively.

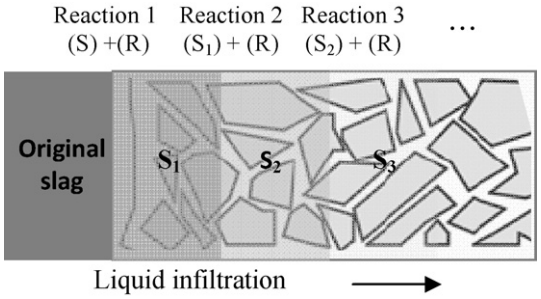

Fig. 1. Sketch of the liquid composition changes after reaction with the refractory material.

$(S) + (R) = 1$. This simulation model provides important information and can be very useful to evaluate complex materials. However, the saturation of the slag in one of its components and its chemical composition change, after the reaction with the refractory, are not considered in this approach.

Thus, in this work a novel modeling is proposed and iterative calculations were applied, considering the liquid composition changes. A sketch of this model is shown in Fig. 1. Firstly, 100 g of each designed castables and 100 g of a slag composition (comprised of a mixture of 90 wt% of an industrial secondary metallurgy slag – Table 2 – and 10 wt% of Fe_2O_3) were considered in the first reaction stage between these two materials. All calculations were performed for a constant temperature of 1550 °C and pressure of 1 atm. After the first reaction step, the resulting liquid slag (S_1) was again put in contact with the same amount (100 g) of the original castable composition used before and a further thermodynamic calculation was carried out. This procedure was constantly repeated and in order to define at which point (step) the calculations should end, some predictions of the phases contained in the castable samples thermally treated at 1500 °C were also performed in the FactSage software. The attained results (amount of the main solid phases of the fired castables) were considered as the target to be reached in an equilibrium condition, considering that all the possible reactions involving liquid and solid phases were completed. Thus, the slag–refractory simulations were carried out until the calculated amount of the main solid phases (after all the possible reactions) attained the same values of the ones predicted for the fired compositions.

After that, the changes in the amount of the phases (predicted by the thermodynamic simulations) formed during the interaction of the liquid with the castables were compared with those obtained in some corrosion cup-tests.

Further calculations to define the free Gibbs energy of some reactions and equilibrium predictions (aiming to verify the slag and refractories' phase compositions separately) were performed to better explain the corrosion mechanisms of the castables.

2.3. Corrosion tests

During the preparation of the samples, a total of 0.2 wt% of a polycarboxylate-based dispersant was added to the suspensions (Bayer, Germany) in order to ensure a good dispersion of the fine particles. The water contents for a suitable vibratable shaping were in the range of 3.9–4.1 wt% for the IS-6C1S, IS-6C0S and PF-6C1S (cement-containing compositions) and 5.3 wt% for the hydratable alumina containing castable (IS-6H1S). After mixing, the prismatic samples used in the corrosion tests (150 mm × 25 mm × 25 mm) were molded, cured at 50 °C for 24 h, dried at 110 °C for 24 h and pre-fired for 5 h at 600 °C. Before the corrosion experiments, the prepared samples were also thermally treated at 1500 °C for 5 h, in order to ensure the formation of *in situ* spinel and calcium hexaluminate (CA_6) in the castable microstructure.

Table 2
Chemical composition of the industrial secondary metallurgy slag used in this work.

Composition	Al_2O_3	MgO	CaO	SiO_2	MnO	Fe_2O_3
wt%	29.6	3.1	44.9	5.3	2.2	4.9

After that, small cups were drilled into the fired samples (central inner diameter of 10 mm and 10 mm deep), which were filled with a mixture of 90 wt% of the slag (Table 2) and 10 wt% of iron oxide. The corrosion cup tests were conducted in a vertical tube furnace in a controlled oxidizing atmosphere (oxygen partial pressure = 0.21 atm) (HTRV 100-250/18 GERO) at 1550 °C for 2 h. The corroded samples were also cut and their cross sections were polished for scanning electron microscopy (JEOL JSM-5900 LV, The Netherlands) evaluation.

3. Results

3.1. Thermodynamic simulation

The phase evolution for each system at different steps of calculation is plotted in Fig. 2. As the slag reacts with the designed spinel containing castables, the composition of the liquid (SLAG) changes up to its saturation until the stage where the thermodynamic results show that the refractories should not be chemically further attacked by the slag. This condition (which corresponds to the end of the solid dissolution) is only observed when the content of the main phases of the reacted castable composition (after interaction with the slag) is similar to the ones attained for the castable samples treated at 1500 °C for 5 h (before slag contact). Thus, the composition shown at the right corner of the figure (stated as a castable) is related to the fired castable composition attained by thermodynamic simulation, disregarding the minor components (i.e., mullite predicted in the IS-6H1S material) and the liquid phases containing silica in the IS-6C1S and PF-6C1S, as they were incorporated by the slag during the corrosion process. It is important to point out that the FactSage predictions of the phases contained in the fired samples are in agreement with the quantitatively XRD analyses of these castables (results not shown here).

For the four different compositions, new phases were formed between the slag and the castable indicating that corrosion was carried out by an indirect mechanism, which corresponds to the

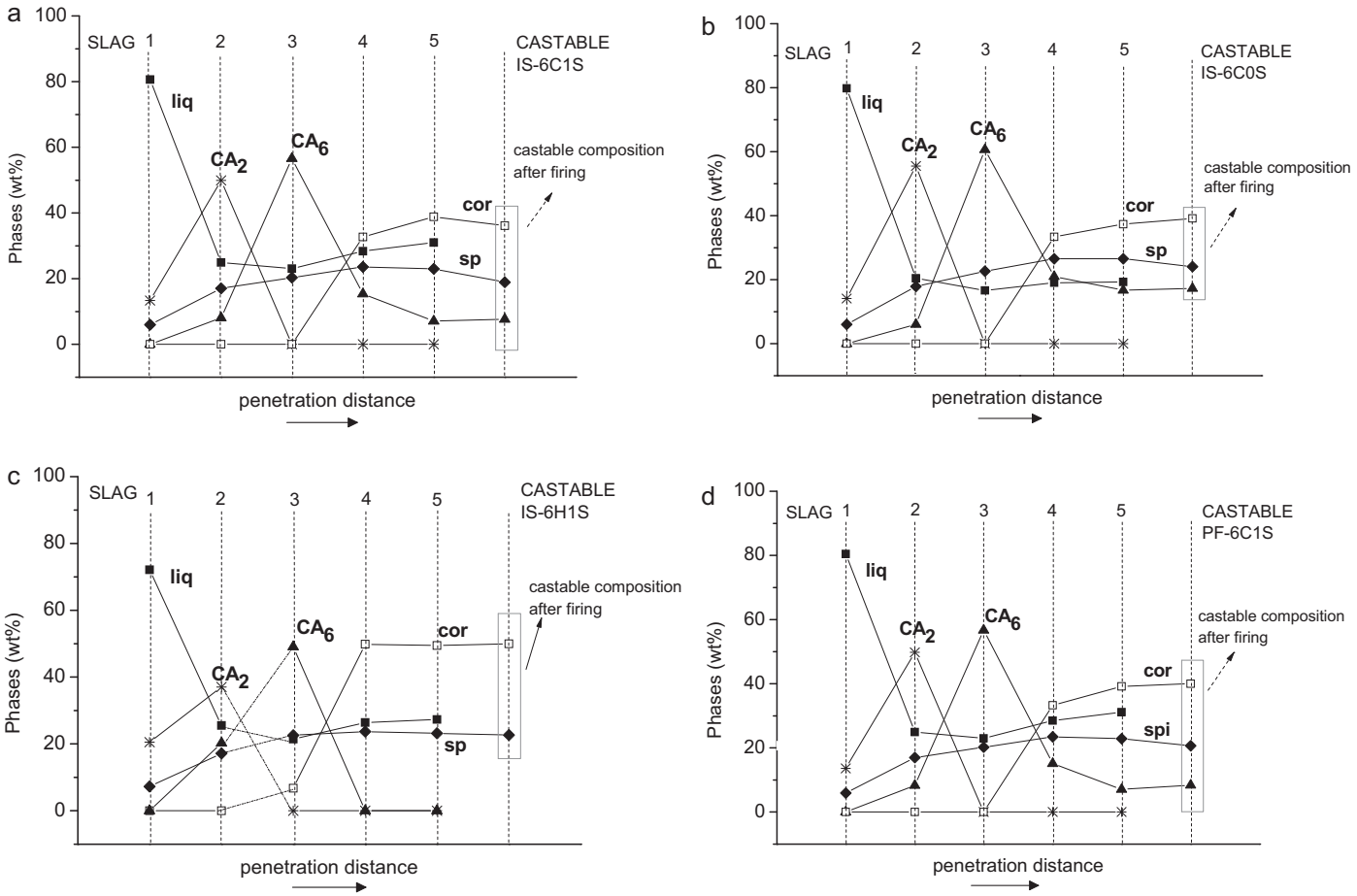

Fig. 2. Phase evolution predicted by the thermodynamic simulations for the corroded spinel containing castables (a) IS-6C1S, (b) IS-6C0S, (c) IS-6H1S and (d) PF-6C1S. The straight lines connecting the points are just to guide the eyes.

dissolution of the refractory and precipitation of new solid phases (such as CA_2, CA_6 and spinel) [7–9,15]. Due to this aspect, the outcome would be a final layered microstructure, as previously reported in similar systems [13,14]. These layers are a consequence of the liquid saturation by the castable components, resulting in the formation of new phases as the interaction slag–castable takes place. Considering the composition IS-6C1S as a reference for the analyses, the following sequence is observed in Fig. 2a:

- *Step* 1: in the first contact between the slag and the refractory, the total or partial dissolution of the main phases of the castable occurs. Consequently, at this point, the alumina from the aggregates and the CA_6 found in the castable matrix and/or on the aggregate surfaces is completely dissolved, as their values are null. On the other hand, the spinel presented in the castable microstructure might also be attacked by the slag at 1550 °C (because its content is lower than the one predicted for the fired castable sample) and, after the MgO dissolution from the castable; enriching the slag with this oxide; $MgO{\cdot}Al_2O_3$ is likely to be generated as shown in Eq. (1)

$$MgO_{(l)} + Al_2O_{3(l)} \rightarrow MgO^{\bullet}Al_2O_{3(s)} \quad (1)$$

After the total (Al_2O_3, CA_6) and partial (spinel) dissolution, CA_2 is predicted to be the first new phase to be formed at the interface between the slag and the castable IS-6C1S. The possible reactions which can take place at 1550 °C and result in the CA_2 generation are:

(a) CA_6 reaction with $CaO_{(l)}$

$$CA_{6(s)} + 2CaO_{(l)} \rightarrow 3CA_{2(s)}, \quad \Delta G_{1550\,^{\circ}C} = -65.1\,\text{kJ/mol} \quad (2)$$

(b) Precipitation from the liquid phase

$$2Al_2O_{3(l)} + CaO_{(l)} \rightarrow CA_{2(s)}, \quad \Delta G_{1550\,^{\circ}C} = -152.2\,\text{kJ/mol} \quad (3)$$

Regarding the thermodynamic equilibrium, the reaction involving only products coming from the liquid (Eq. (3)) presented the more negative Gibbs free energy and, consequently, is more likely to occur in this condition.

- *Step* 2*:* in this calculation step, the remaining liquid of the first reaction between the slag and the refractory is placed again in contact with the same amount used before (100 g) of the original castable composition. After the possible reactions and at the equilibrium condition, the major predicted phases are the CA_2 (which increases and reaches

a maximum value at this point) and the liquid derived from the Al_2O_3, CA_6 and spinel dissolution. CA_6 and spinel are also present in proportions slightly lower than those of the fired refractory. This fact could indicate that these phases remained from the original castable, even though it cannot be disregarded that new crystals were formed after the slag attack. The crystallization of new grains of spinel is likely to occur by precipitation from the liquid, as previously presented in Eq. (1). However, the CA_6 generation is expected to take place by:

(a) The reaction of CA_2 with $Al_2O_{3(l)}$ (in this zone, all solid Al_2O_3 of the castable should be dissolved into the liquid slag)

$$4Al_2O_{3(l)} + CA_{2(s)} \rightarrow CA_{6(s)} \quad \Delta G_{1550\,^{\circ}C} = -109.0\,\text{kJ/mol} \tag{4}$$

(b) The precipitation from the liquid

$$6Al_2O_{3(l)} + CaO_{(l)} \rightarrow CA_{6(s)} \quad \Delta G_{1550\,^{\circ}C} = -261.1\ \text{kJ/mol} \tag{5}$$

Again, the reaction involving the liquid reagents (Eq. (5)) is more likely considering the thermodynamic equilibrium. The generation of CA_2 and CA_6 followed by spinel is also reported by other authors who investigated the corrosion of spinel containing castables via thermodynamic simulations [14]. However, they considered a different modeling approach without taking into account the changes of the slag composition.

- *Step* 3: following the calculation procedure, the liquid attained in the second step reacted again with the original composition of the IS-6C1S castable. At equilibrium, the complete dissolution of the Al_2O_3 is detected and the weight percentage of CA_2 drops to zero at a certain distance of slag penetration into the refractory. The amount of CA_6 reaches its maximum value (56.6 wt%) and the spinel content also slightly increases to a value higher than the one predicted for the fired castable, indicating that new crystals are formed according to the mechanisms proposed in Eq. (1).
- *Step* 4: corundum is identified as the major phase at this calculation step, which is an indicative that not all alumina of the IS-6C1S was dissolved into the slag at the equilibrium condition. A small amount of CA_6 is formed (11.2 wt%, comparing with the original amount (7.1 wt%) contained in the fired sample) resulting in a total of 18.3 wt% after the slag–castable interaction, most likely due to the previous consumption of CaO from the liquid according to the simulations evaluated before. Furthermore, the liquid and spinel contents increased slightly after all the possible transformations
- *Step* 5: few changes of the CA_6, spinel and corundum contents are observed at this point when compared with the fired castable. Thus, the thermodynamic simulations were conducted up to this step

According to these results, as the slag penetration advances into the IS-6C1S castable, the solid phases are found in the following sequence:

$$\text{slag}//CA_2 + \text{spinel}/CA_2 + \text{spinel} + CA_6/CA_6 + \text{spinel}/\text{cor.} + \text{spinel} + CA_6//\text{castable}$$

The first component of each step of the sequence presented above corresponds to the phase which had the highest content in the calculated results. Among the formed phases, some of them correspond to non-stoichiometric solids. This effect is not only observed for the spinel, but also in the calcium aluminates (CA_2 and CA_6 which incorporate mainly Fe_2O_3 into their solid solutions) and the corundum (which contains Fe_2O_3 and Mn_2O_3 in its composition).

The liquid slag (which is in equilibrium with the solid phases) showed a significant drop in its content in step 2 due to the formation of some crystalline phases (CA_2, CA_6 and spinel). After that, the amount of liquid increased slowly (step 4), although it did not reach the previous levels. In order to better evaluate the evolution of the oxide components of the liquid slag, the composition of the liquid was plotted for the IS-6C1S castable (Fig. 3a and b).

According to these graphs, the formation of calcium aluminates from the liquid components was consistent with the decrease in the mass of alumina and calcia up to the point where the content of CA_6 reached the value predicted for the fired refractory (step 5). Additionally, the evolution of the oxides contents in the liquid indicates its silica enrichment (Fig. 3a). At the first contact between the slag and the refractory at 1550 °C, the silica containing phases of the castable are incorporated by the liquid. This fact confirms the easier dissolution of the silicate phases present in the fired refractory and, as the slag penetration advances, the amount of silica in the slag composition increases continuously up to 10.3 g (~22.3 wt%), indicating that at each calculation step 1 g of SiO_2 (amount of silica fume added to the IS-6C1S composition, considering a 100 g sample) was incorporated by the liquid.

The MgO profile follows the spinel crystal formation. After an initial increase in the MgO content (step 1) due to the dissolution of spinel, a reduction was detected, as the spinel became more stable and even new crystals of this phase might have been formed. The iron content in the liquid decreased according to the formation of solid phases (CA_2, CA_6, spinel and corundum) and the incorporation of Fe^{2+} and Fe^{3+} into the solid solution. However, the Mn^{2+} showed an initial reduction of its content, followed by an increase (Fig. 3b). This aspect could indicate lower solubility of this cation in the phases formed at these steps (i.e., corundum).

After presenting the main results in detail of the IS-6C1S castable corrosion predicted by the thermodynamic simulation, the following paragraphs discuss the differences observed for the IS-6C0S, IS-6H1S and PF-6C-1S calculations. The evaluation of these compositions aimed to analyse the effect of silica fume, the binder source (calcium aluminate cement – CAC – or hydratable alumina – HA) and also the spinel incorporation method (*in situ* versus pre-formed for compositions containing CAC and silica fume).

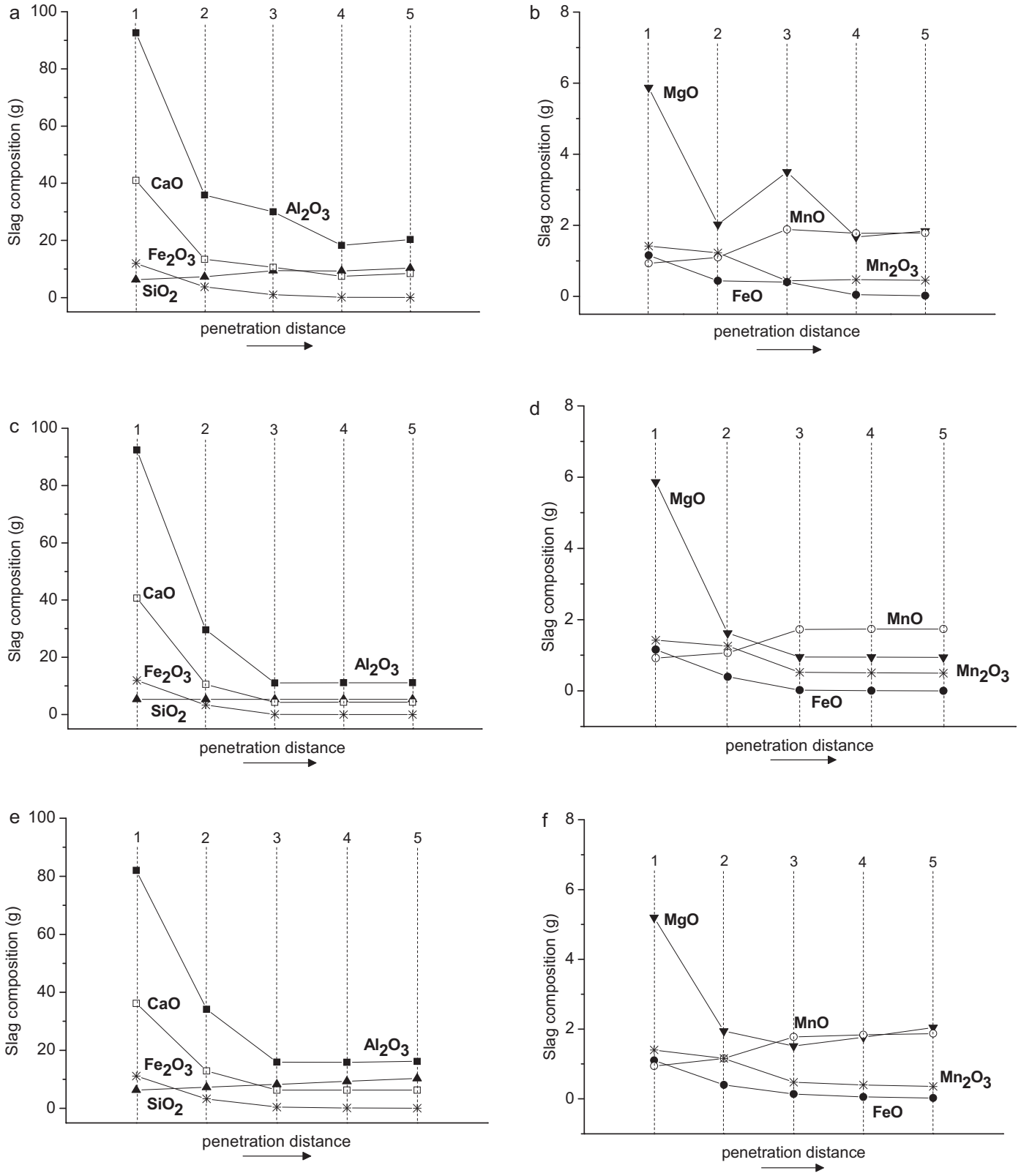

Fig. 3. Thermodynamic predictions for the liquid composition attained after the slag–refractory interaction. (a and b) IS-6C1S, (c and d) IS-6C0S and (e and f) IS-6H1S.

The corrosion of the IS-6C0S (containing CAC and no silica fume) and the IS-6H1S castable (which comprises HA instead of CAC) did not show marked differences when compared to those calculated for IS-6C1S. The predicted phases were qualitatively similar and the same sequence and reaction mechanisms to those of IS-6C1S were attained (Fig. 2b and c). This fact is associated to the similarities in the chemical compositions (expressed as oxides) of the designed spinel

containing refractories, which is the input data for the calculation (as in every estimation based on the equilibrium phase diagrams). Consequently, the results of the phase evolution of the pre-formed spinel containing composition (PF-6C1S) are the same as those reported for IS-6C1S (as shown in Fig. 2d), because the simulation disregards the way in which those oxides are combined, as well as other physical and microstructural aspects, considering only the overall chemical composition.

Nevertheless, some differences were observed in the calculation results of the IS-6C0S and IS-6H1S castables (Fig. 2b and c):

- The amount of liquid in these compositions is lower than in IS-6C1S (around 30% less liquid after step 3) due to the absence of silica fume (IS-6C0S) and cement (IS-6H1S). Moreover, the content of CA_6 is in general higher in the composition IS-6C0S.
- The initial CA_2 content, after the first contact with the slag (step 1, Fig. 2c) is higher in IS-6H1S than in the other systems. In agreement with this aspect, the amount of Al_2O_3 and CaO present in the liquid is slightly lower after the first reaction (Fig. 3e).
- The earlier detection of corundum in the IS-6H1S (step 3, Fig. 2c) when compared to other analysed castables can also be highlighted. This feature has an apparent thermodynamic incompatibility because CA_2 and corundum appear to co-exist in equilibrium when the points plotted in the graph (Fig. 2c) are joined using straight lines. According to the equilibrium phase diagram of the system SiO_2–CaO–Al_2O_3, the simultaneous presence of CA_2 and Al_2O_3 is incompatible and these phases should react forming CA_6 [7]. However, it must be pointed out that none of the simulation resulted in the co-existence of CA_2 and Al_2O_3. This incompatibility is only apparent and the joint points between the simulation steps 2 and 3 are highlighted with a dotted line.

It must also be pointed out that the amount of silica in the liquid attained after the corrosion of the IS-6C0S castable (Fig. 3c and d) is always constant, in contrast with the results observed for the IS-6C1S, when the SiO_2 content continuously increases as the silicate phases of the refractory are dissolved. The $Al_2O_{3(l)}$ and $CaO_{(l)}$ contents also tend to stabilize earlier (step 3, Fig. 3c) and at lower values than in the IS-6C1S, which is in agreement with the higher amount of CA_6 present in the IS-6C0S.

Additionally, in order to obtain further thermodynamic data to compare with the experimental corrosion results and better understand the slag phases prone to be formed during the cooling down of the system, the composition of the slag (without any interaction with the spinel containing refractories) was simulated at temperatures lower than that of the corrosion test, 1100 °C and 900 °C. According to these results, calcium aluminates containing iron in their solid solution (CA_2, CA and C_3A), some oxides (MgO, MnO and Fe_2O_3), $CaSiO_4$ (only at 1100 °C) and $MgO{\cdot}Al_2O_3$ (containing 88 wt% of $MnMn_2O_4$ in its solution) might be formed in the slag during cooling, if no reaction with the refractory takes place. For temperatures below 900 °C, no further changes are considered to occur. These results are important to highlight the presence of some phases identified by SEM/EDS, when analysing the corroded cross-section area of the spinel containing castable samples, as will be discussed below.

3.2. Corrosion tests

The cross sections of the castable samples after the corrosion tests and SEM images of the infiltrated zones are shown in Figs. 4 and 5, respectively. Remaining slag was observed at the bottom of the internal cup of the castable samples, except for the PF-6C1S composition. Castable IS-6C1S showed slight dimensional deformation of its original shape, a visible slag penetration and the presence of macroscopic cracks. On the other hand, the greater slag penetration in the PF-6C1S castable (which contained pre-formed spinel) induced a major deformation of this sample and a high level of macrocracking. Moreover, for this composition (PF-6C1S), the tabular alumina aggregates were clearly identified, indicating a remarkable corrosion of the matrix. Castables IS-6C0S and IS-6H1S showed a higher corrosion resistance and no cracks at the samples cross section were detected. Nevertheless, the IS-6C0S composition showed a higher slag penetration than the castable with HA as a binder.

These data indicate differences in the behavior of the castables during the slag corrosion attack. Therefore, although the same slag was used for all tests and the thermodynamic results showed minor differences during the evolution of the phases with the slag penetration, the final microstructure of the corroded castables (Fig. 5) was considerably different for each case. Except for the IS-6H1S, the presence of continuous and well defined layers of calcium aluminates at the edge of the tabular alumina aggregates was observed.

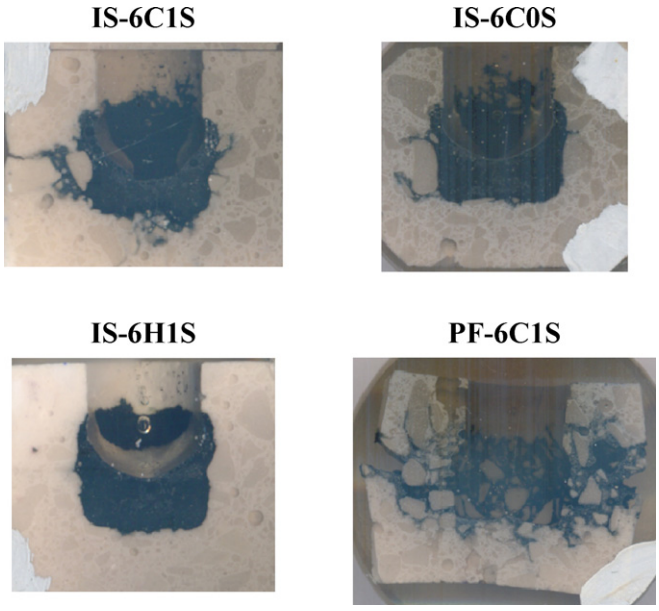

Fig. 4. Cross sections of the corroded samples.

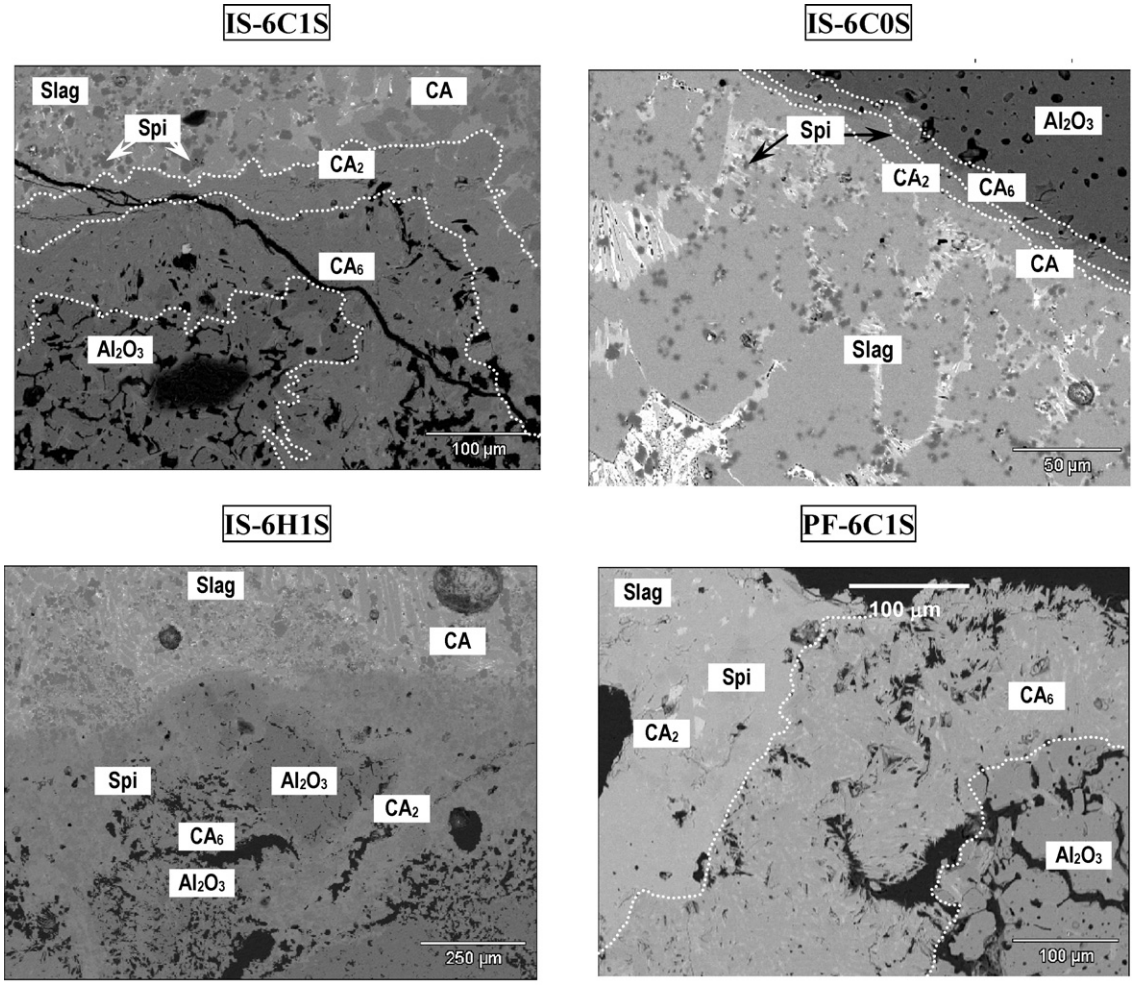

Fig. 5. SEM images of the corroded spinel containing castables (slag–refractory interface).

According to the SEM/EDS analysis, the sequence of formed phases at the interface between the slag and the castables (IS-6C1S, IS-6C0S and PF-6H1S) was:

$$\text{slag}//\text{CA} + \text{spinel}/\text{CA}_2 + \text{spinel}/\text{CA}_6 + \text{spinel}//\text{castable}$$

where, the presence of CA_6 + spinel were not easily detected in the microstructure of the samples. For the IS-6H1S, even when the formation of layers around the alumina aggregates was not clearly observed, the same phases presented above were identified (Fig. 5). It was also detected that calcium aluminates (mainly CA_2 and CA_6) and spinel solid solutions presented some iron content in their compositions (>2 wt% for CA_2 and CA_6 and up to 9 wt% Fe_2O_3 for spinel). The crystal morphologies of the formed phases indicate their precipitation from the

Table 3
SEM/EDS slag composition analysis after the corrosion tests.

	IS-6C1S	IS-6C0S	IS-6H1S	PF-6C1S
CA	✓	✓	✓	✓
CA_2	✓			✓
Ghelenite (CA_2S)	✓			
Ghelenite or glassy phase		✓	✓	✓
C_2A_4S	✓			
Glassy phase	✓			
C_xA_y[a] with Fe_2O_3 or CA with Fe_2O_3 ss		✓	✓	
C_3A c/Fe_2O_3		✓		
C_2F c/A_2O_3 ss			✓	
Spinel	✓	✓	✓	✓
Fe_2O_3	✓			
Oxides mixture[b]		✓	✓	✓

[a] C_xA_y could be: $C_{12}A_7$, C_2A or C_3A.
[b] IS-6C0S and IS-6H1S: MgO + MnO + Fe_2O_3; PS-6C1S: MgO + Al_2O_3 + Fe_2O_3 + CaO.

liquid. The presence of platelet CA_6 grains, cubic-shaped spinels and the formation of a compact layer of CA_2 were detected at the slag–refractory interface.

The slag composition also showed some differences among the evaluated castables after the corrosion tests (Fig. 5). Table 3 presents some of the phases identified in the slag region. Several calcium aluminates, calcium aluminosilicates, oxides, solid solutions, among others, were detected. Based on these results, the experimental and the thermodynamic predictions of the slag phases after cooling down will be compared and discussed in the following section.

4. Discussion

4.1. Thermodynamic simulation

Regarding the evaluation of the thermodynamic results and aiming to define some parameters to explain the slight differences among the predicted corrosion behavior of the spinel containing compositions, the following criteria are proposed:

- *The liquid content generated after the slag-refractory interaction*. The higher the liquid content generated after the reaction between the slag and the castable, the higher the likelihood for penetration in the refractory. Therefore, greater corrosion and solid dissolution would take place. Considering this aspect and in order to analyse the liquid content as a function of the penetration distance, Fig. 6 is presented. The IS-6C0S castable resulted in the lowest liquid content after all the possible reactions at 1550 °C. This is an indicative that the absence of silica fume could inhibit the wearing. Conversely, the other castable compositions (IS-6C1S, IS-6H1S and PF-6C1S, all of them containing 1 wt% of silica fume) showed higher liquid contents due to the dissolution of the phases containing silica (i.e., mullite, saphirine, etc., which are formed in the castables microstructure during the first thermal treatment up to 1500 °C) by the slag. Therefore, according to the thermodynamic predictions, the following ranking for the corrosion resistance is expected: IS-6C0S > IS-6H1S > IS-6C1S = PF-6C1S.
- *The silica content in the liquid composition after the slag–refractory interaction.* Taking into account that a higher amount of SiO_2 leads to higher viscosity of the resulting liquid at 1550 °C, one should expect that the slag penetration would be lower for the silica containing castables. The silica content in the liquid is highlighted in Fig. 7a. The liquid derived from the reactions between the slag and the IS-6H1S composition presented the highest amount of SiO_2 in its composition, followed by the predictions for the IS-6C1S = PF-6C1S and IS-6C0S refractories. Additionally, the viscosity of the resulting liquid at 1550 °C was estimated using the modified Urbain model (which assumes that all oxides change the liquid viscosity depending only on their own content) [16] (Fig. 7b). The correlation between the SiO_2 content and its effect on the liquid viscosity show that, after some thermodynamic calculation steps, the slag viscosity of the IS-6H1S castable is higher than the other studied systems. Based on this information, the refractory which comprises

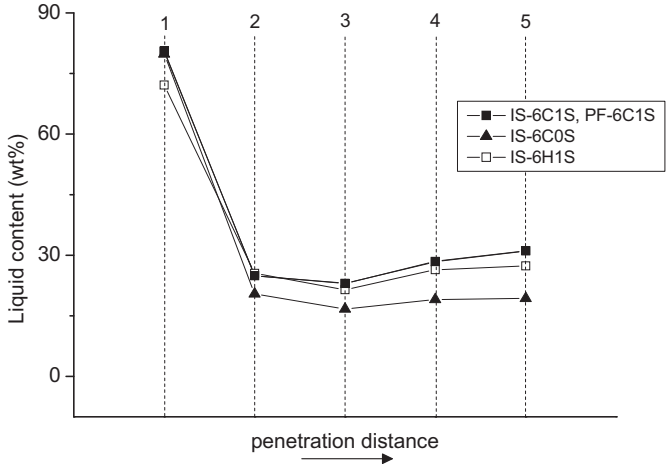

Fig. 6. Thermodynamic predictions of the liquid content, at 1550 °C, after the slag–castable reaction steps as a function of the penetration distance.

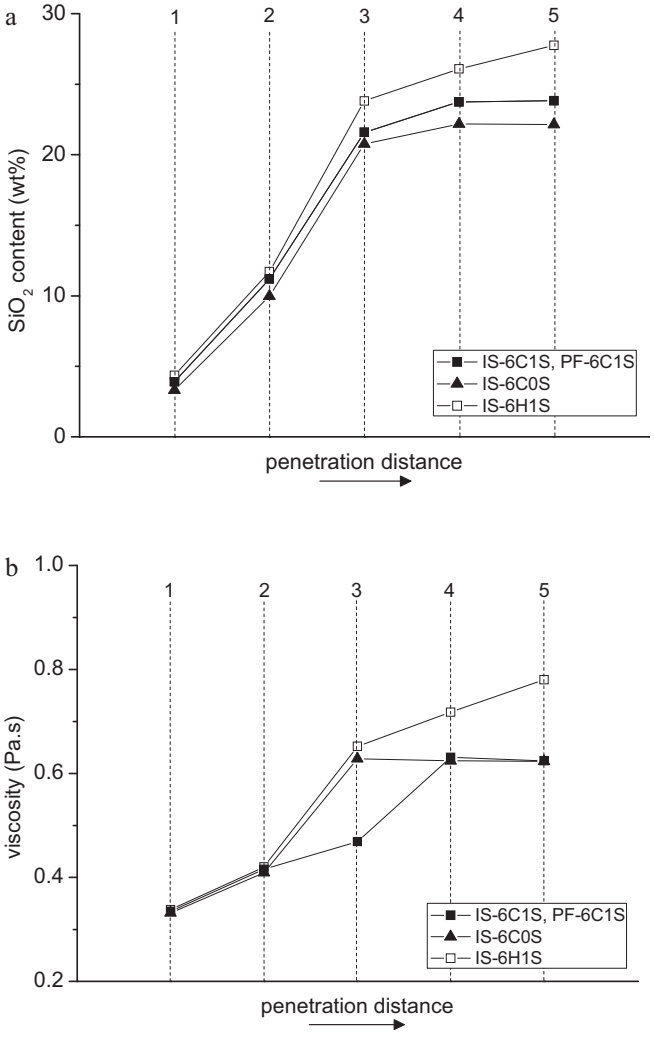

Fig. 7. Thermodynamic predictions of the (a) silica content in the resultant liquid after the slag–castable reactions and (b) its viscosity at 1550 °C.

hydratable alumina as the binder source and 1 wt% of silica fume should present the highest slag penetration resistance.

- *The presence of corundum.* The earlier this phase is identified, the more corrosion resistant the refractory should be. In other words, after the initial slag–refractory contact, all the alumina from the refractory is dissolved into the liquid (Fig. 2, corundum content is zero at step 1). However, as the slag infiltrates the refractory, corundum might be present due to the saturation of the slag and no more dissolution of this phase is expected to occur. Afterwards, the amount of this solid phase increases up to the content of the original refractory. For the IS-6H1S simulation, the corundum phase was detected in an earlier step than in the other castables. This result is associated with the higher supply of Al_2O_3 in this system. Following this criteria, the corrosion resistance of the designed spinel castables should be: IS-6H1S > IS-6C1S, IS-6C0S, PF-6C1S.

According to the statements above and assuming that all of them are equally important, the castable that should have the highest corrosion resistance is the IS-6H1S. This composition presented a relatively low liquid content with the highest viscosity and a higher resistance to dissolve alumina. The castable with no silica fume (IS-6C0S) has the advantage of presenting the lower liquid content after various reaction steps, which could be an indicative of its good performance during the corrosion test. Additionally, considering the thermodynamic calculations, the slag attack and the corrosion behavior of the IS-6C1S and PF-6C1S is similar, although the spinel incorporation method (*in situ* versus preformed, respectively) should directly affected the corrosion cup-test performance of these materials. The physical differences among these compositions and the different corrosion behavior will be presented in a forthcoming publication by the authors.

4.2. Comparison between experimental and thermodynamic simulation data

The similarities of the phases predicted by the thermodynamic simulation for the four castables are associated to the assumptions of the model used to calculate the slag–refractory interaction. Although it represents an advance regarding the models used up to now, it disregards important aspects that also affect the corrosion behavior. The use of the overall chemical composition of the castables does not take into consideration physical parameters such as the granulometric differences between the aggregates and the matrix, the location of these phases in the refractory microstructure and the castable open porosity and permeability. These aspects affect the behavior of the material as the finer matrix dissolves easily, modifying the slag composition.

However, the thermodynamic simulation is suitable for predicting the sequence of phase transformations in equilibrium (generation of CA_2, CA_6 and spinel phases at the interface between the slag and the refractory). Spinel and calcium aluminates were clearly detected in the corroded castable samples by the SEM/EDS analyses (Fig. 5) and, except for the IS-6H1S composition, all the refractories presented well defined layers of CA_6 and CA_2 at the edge of tabular alumina aggregates. The absence of CaO in the IS-6H1S matrix (cement free composition) is most likely the main reason for this distinct behavior, because calcium would be only provided by the slag.

Besides CA_2 and CA_6, calcium mono-aluminate (CA) was also observed at the slag–refractory interface, as shown in Fig. 5 (except for the castable PF-6C1S that only showed CA crystals in the slag). A possible explanation based on the equilibrium calculations is that this phase is formed when cooling (from 1550 °C to room temperature), as confirmed by the results attained during the evaluation of the slag phases formed at lower temperatures (1100 °C and 900 °C). Additionally, the CA generation could be related to a lack of fine alumina supply, inhibiting further CA_2 and CA_6 formation.

The CA_2 phase, presented in the IS-6C1S, IS-6C0S and PF-6C1S compositions, was identified by SEM as a compact layer with low porosity. As predicted by Eq. (3) this phase should be precipitated from the liquid, resulting in a dense and organized structure at the slag–refractory interface. According to the phase transformations of the Al_2O_3–MgO–CaO systems [17], at 1100 °C, calcium di-aluminate (CA_2) can be formed by the reaction between CA and alumina. Some authors also inferred experimentally that CA_2 is the first solid phase generated at the refractory surface during the corrosion process [7], confirming the results attained in the simulations.

At 1450 °C, CA_2 and $Al_2O_{3(s,l)}$ or calcium and alumina from the liquid can react forming CA_6 [17]. A dense layer of CA_2 and CA_6 in the IS-6C0S microstructure samples indicates that this phase might be a product of the reaction involving liquid reagents. The smaller thickness of these calcium aluminate layers around the alumina aggregates is also associated to the lower liquid content, as estimated by the simulation for this castable composition. On the other hand, the reaction of $CA_{2(s)}$ and alumina (forming CA_6) should result in a porous network of interlocked platelets [17], as detected by SEM for PF-6C1S and IS-6C1S compositions (Fig. 5), which suggests that its formation also involves the tabular alumina aggregates as the alumina source.

Concerning the iron and manganese inclusions, a small content of Fe_2O_3 and Mn^{2+}/Mn^{3+} was also detected in the calcium aluminates (CA, CA_2 and CA_6) solid solutions by the chemical analysis (EDS) of the corroded castables (Table 3). These results are in agreement with the FactSage predictions which considered the formation of non-stoichiometric phases (spinel, calcium aluminates and corundum) containing Fe^{2+}, Fe^{3+}, Mn^{2+} and/or Mn^{3+} as minor components.

Furthermore, the morphology of the spinel, CA_6 and CA_2 phases observed in the corroded samples (Fig. 5) also indicates that they have been formed in the presence of liquid, in agreement with the Gibbs free energy values for these transformations (Eqs. (1), (3) and (5)) [14,15].

Considering some factors, such as: the remaining slag inside the internal cup of the samples after the corrosion tests, the slag penetration, the samples deformation, and the formation of macrocracks; a ranking, defining which composition presented the best corrosion resistance behavior after the experimental evaluation, can be drawn up as follows: IS-6H1S > IS-

6C0S > IS-6C1S > PF-6C1S. This relative order agrees with the ranking predicted by the thermodynamic simulation according to the criteria previously established (the liquid amount, the viscosity of the liquid and the presence of corundum).

The agreement of various aspects of the corrosion behavior predicted by the thermodynamic simulation shows the usefulness of this tool for supporting experimental results, despite the constraints imposed by the assumed simplifications. Moreover, the possibility of reducing the number of experimental tests is especially attractive in the study of refractory corrosion.

However, further improvements can still be implemented in the modeling procedure which would result in a better agreement between the theoretical and experimental results. In this context, an alternative would be to develop calculations considering previous interaction of the slag liquid with the matrix compounds and later with the aggregates.

5. Conclusions

The corrosion of four spinel containing refractory castables was evaluated in this work by thermodynamic simulations and corrosion cup-tests and based on the attained results, the following conclusions can be drawn:

- The main transformations and the sequence of the chemical reactions (formation of CA_2, CA_6 and spinel) that take place at the slag–refractory interface were correctly predicted by the calculations and confirmed by the experimental analyses of the corroded samples.
- The thermodynamic results pointed out that the addition of silica to the spinel containing castables increase the liquid content after the slag–refractory interaction due to the easier incorporation of the silica containing phases by the slag.
- Although the silica fume addition affected the corrosion resistance of the castables negatively due to the liquid generation at a high temperature, it also increased the viscosity of the slag, resulting in the highest slag penetration resistance for the IS-6H1S composition (cement free refractory).
- The binder source had a significant effect on the slag saturation and the formation of the calcium aluminate phases at the castables interface. According to the predictions, the IS-6H1S (containing 6 wt% of hydratable alumina instead of cement) was the only material that presented corundum at a position closer to the slag zone, indicating the requirement of lower dissolution of this phase to attain the thermodynamic equilibrium.
- A ranking, defining which composition presented the best corrosion resistance behavior after the experimental evaluation, was drawn up as follows: IS-6H1S > IS-6C0S > IS-6C1S > PF-6C1S. This relative order agrees with the simulation results according to the criteria previously established (the liquid amount, the viscosity of the liquid and the presence of corundum).

In order to better explain the physical differences among these castable compositions and the distinct observed corrosion behavior, a detailed analyses and discussion of the experimental aspects will be presented in a forthcoming publication by the authors.

Acknowledgments

The authors are grateful to the Federation for International Refractory Research and Education (FIRE), Magnesita Refratários S. A. (Brazil), FAPESP and CNPq. Additionally, the authors are thankful to the Corus Ceramic Research Centre (CRC) for the microstructure evaluation and corrosion test support.

References

[1] P. Korgul, D.R. Wilson, W.E. Lee, Microstructural analysis of corroded alumina–spinel castable refractories, J. Eur. Ceram. Soc. 17 (1997) 77–84.
[2] Y. Ko, Influence of the characteristics of spinels on the slag resistance of Al_2O_3–MgO and Al_2O_3–spinel castables, J. Am. Ceram. Soc. 83 (2000) 2333–2335.
[3] H. Sarpoolaky, S. Zhang, W.E. Lee, Corrosion of high alumina and near stoichiometric spinels in iron-containing silicate slags, J. Eur. Ceram. Soc. 23 (2003) 293–300.
[4] S. Yilmaz, Corrosion of high alumina spinel castables by steel ladle slag, Ironmaking Steelmaking 33 (2) (2006) 151–156.
[5] L.A. Díaz, R. Torrecillas, A.H. de Aza, P. Pena, Effect of spinel on slag attack resistance of high alumina refractory castables, J. Eur. Ceram. Soc. 27 (2007) 4625–4631.
[6] S. Mukhopadhyay, T.K. Pal, P.K. DasPoddar, Improvement of corrosion resistance of spinel-bonded castable to converter slag, Ceram. Inter. 35 (2009) 373–380.
[7] J.P. Guha, Reaction chemistry in dissolution of polycrystalline alumina in lime–alumina–silica slag, Br. Ceram. Trans. 96 (6) (1997) 231–236.
[8] S. Zhang, H.R. Rezaie, H. Sarpoolaky, W.E. Lee, Alumina dissolution into silicate slag, J. Am. Ceram. Soc. 83 (4) (2000) 897–903.
[9] H. Sarpoolaky, S. Zhang, B.B. Argent, W.E. Lee, Influence of grain phase on slag corrosion of low-cement castable refractories, J. Am. Ceram. Soc. 84 (2) (2001) 426–434.
[10] M. Fuhrer, A. Hey, W.E. Lee, Microstructural evolution in self-forming spinel/calcium aluminate-bonded castable refractories, J. Eur. Ceram. Soc. 18 (1998) 813–820.
[11] K. Goto, B.B. Argent, W.E. Lee, Corrosion of MgO–$MgAl_2O_4$ spinel refractory bricks by calcium aluminosilicate slag, J. Am. Ceram. Soc. 80 (2) (1997) 461–471.
[12] C.W. Bale, P. Chartrand, S.A. Degterov, G. Eriksson, K. Hack, R. Ben Mahfoud, J. Melançon, A.D. Peltron, S. Petersen, FactSage thermochemical software and databases, Calphad 26 (2) (2002) 189–228.
[13] J. Poirier, M.L. Bouchetou, P. Pringent, J. Berjonneau, An overview of refractory corrosion: observations, mechanisms and thermodynamic modeling, Refractories Appl. Trans. 3 (2) (2007) 2–12.
[14] J Berjonneau, P. Pringent, J. Poirier, The development of a thermodynamic model for Al_2O_3–MgO refractory castable corrosion by secondary metallurgy steel ladle slags, Ceram. Int. 35 (2) (2009) 623–635.
[15] W.R. Lee, S. Zhang, Melt corrosion of oxides and oxide–carbon refractories, Int. Mater. Rev. 44 (1999) 77–104.
[16] G.J. Browning, G.W. Bryant, H.J. Hurst, J.A. Lucas, T.F. Wall, An empirical method for the prediction of coal ash slag viscosity, Energy Fuel 17 (2003) 731–737.
[17] J.M. Auvray, C. Gault, M. Huger, Microstructural changes and evolutions of elastic properties versus temperature of alumina and alumina–magnesia refractory castables, J. Eur. Ceram. Soc. 28 (2008) 1953–1960.